JOURNAL OF THERMOPHYSICS AND HEAT TRANSFER
Vol. 6, No. 2, April–June 1992

Steady-State Post-Critical Heat Flux Heat Transfer to a Refrigerant

J. M. Paske,* P. Papadopoulos,* C. M. George,* D. M. France,† and W. J. Minkowycz†
University of Illinois at Chicago, Chicago, Illinois 60680

Heat transfer in the post-critical heat flux (CHF) regime was studied experimentally under steady-state conditions producing low superheat temperature of the heated surface. Experiments were performed with the vertical flow of refrigerant-12 in a tube with inside diameter of 7.75 mm over the mass flux range of 182 to 808 kg/m²s at a pressure of 1 MPa. Liquid heating produced the low wall-superheat in the post-CHF region at steady state, which is typical of heat exchanger operation. Superheated vapor measured at the test section exit in most tests ensured that the entire post-CHF region was included. Heat transfer results were compared to predictions from nine post-CHF correlations and models. The potential for thermodynamic nonequilibrium diminishes and direct wall-drop heat transfer is enchanced when wall-superheat is low. These two phenomena were considered in the comparisons, and the best predictions of independent data for two fluids, refrigerant-12 and water, were obtained from a single correlation that included both phenomena explicitly.

Nomenclature

c_p = specific heat, J/kg K
D = diameter, m
G = mass flux, kg/m²s
h = heat transfer coefficient, kW/m²K
i_{lv} = latent heat of vaporization, J/kg
k = thermal conductivity, kW/m K
L_{CHF} = length downstream of CHF, m
m = mass flow rate, kg/s
Nu = Nusselt number
P = pressure, MPa
Pr = Prandtl number (reduced pressure in Fig. 11)
q'' = heat flux to boiling fluid, kW/m²
Re = Reynolds number based on hydraulic diameter
S = slip ratio, V_v/V_l
T = temperature, °C
Tw = wall temperature, °C
V = velocity, m/s
X = quality
Z = axial distance in direction of water flow, m
α = vapor void fraction
Γ = parameter in Eq. (4)
δ = drop diameter, m
μ = dynamic viscosity, kg/m s
ρ = density, kg/m³
σ = surface tension, N/m

Subscripts

a = actual
CHF = critical heat flux
eq = equilibrium
f = film temperature (properties evaluated at bulk temperature unless noted otherwise)
h = heating liquid
i = tube inner surface
l = liquid
o = tube outer surface
s = shell
sat = saturated
v = vapor
w = wall
$w-\delta$ = wall-to-drop
$w-v$ = wall-to-vapor

Received Sept. 14, 1990; revision received March 8, 1991; accepted for publication March 8, 1991.

*Graduate Research Assistant, Department of Mechanical Engineering.
†Professor, Department of Mechanical Engineering.

Introduction

THE transport of discrete liquid drops in a continuous vapor stream constitutes the two-phase flow regime known as film boiling, mist flow, dispersed flow, and post-critical heat flux (post-CHF), and is the subject of this investigation. A significant portion of research performed and experimental data obtained in this area has been for application to nuclear reactor core conditions characterized by high wall-superheats. As a result, many correlations and analyses have been developed to predict heat transfer under this condition. Recent surveys of post-CHF heat transfer were given.[1,2]

Another important application for the post-CHF flow regime occurs in heat exchangers where the wall-superheats are typically very low. Steam generators for use with nuclear reactors and air-conditioning and refrigeration evaporators are examples of such heat exchangers. Two phenomena, important to heat transfer in the post-CHF region, are directly affected by the level of the wall-superheat. These phenomena, of thermodynamic nonequilibrium in the flowstream and the effectiveness of direct wall-drop heat transfer, can be significantly different if the wall-superheat is high (in the range of 200–300°C) or low (less than 100°C). The condition of low wall-superheat minimizes the potential for vapor superheat in the presence of liquid drops and, thus, minimizes the potential extent of nonequilibrium. Low wall temperature increases the effectiveness of wall-drop heat transfer by minimizing the Leidenfrost phenomenon. Because most of the post-CHF research in the engineering literature has been directed toward the high wall-superheat condition, many of the heat transfer models and correlations have neglected the effect of wall-drop heat transfer[3] and recently have included the effect of vapor superheat. Significant differences in these two phenomena at low wall-superheat lead to this investigation, specifically into the low wall-superheat case.

A study[4] was completed in the area of heat transfer in the post-CHF region utilizing low wall-superheat data obtained from experiments[5,6] with water at high pressure (7.0–15.3 MPa) and high mass flux (720–3200 kg/m²s). The data were assessed with cognizance of the importance on the overall

heat transfer of the two phenomena of thermal nonequilibrium and direct wall-drop heat transfer. The data were compared to predictions from 13 correlations, models, and analyses (plus variations of them) representing both equilibrium and nonequilibrium approaches. These models were developed from the available data, which were predominantly for high wall-superheat. In assessing the validity of the predictions at low wall-superheat, it was found[4] that the best results were obtained when both nonequilibrium effects and direct drop-wall heat transfer were included in the model. The Plummer correlation[7] was the most accurate in prediction of the magnitudes and the trends of the data, and several other models considered predicted the magnitudes well.

In this present investigation, the database for low wall-superheat post-CHF heat transfer was extended to lower mass fluxes in the range applicable to once-through heat exchanger operation, to a second fluid, and to qualities beyond unity to include the entire post-CHF region. Experiments were performed in the flow boiling facility (FBF) at the University of Illinois at Chicago using refrigerant-12 (R-12) as the boiling fluid. The mass flux range was 182 to 808 kg/m^{2}s, which overlapped the water data.[5,6] The R-12 pressure was 1 MPa, which simulated the lowest water pressure tested[5,6] of 7 MPa based on equal liquid-to-vapor density ratios of the two fluids. (The reduced pressures of the two fluids had similar values of 0.25 and 0.32 for R-12 and water, respectively.) The post-CHF data were obtained under steady-state conditions with low wall-superheat by using liquid heating of the test section. Further investigation of the important physical phenomena and the accuracy of correlations and models for low wall-superheat post-CHF heat transfer was conducted using correlations[4] shown to be the most accurate with the water data. Data from both of the fluids R-12 and water were compared to these correlations.

Experimental Facility

The FBF is shown schematically in Fig. 1. It consists of two closed pumped fluid circuits for the boiling fluid (R-12) and the heating fluid (water). The liquid heating aspect of the facility is unique; it allows steady-state testing in the post-CHF region under heat exchanger conditions. The liquid heating also provided the low wall-superheat required for this study.

The boiling fluid circuit shown in Fig. 1 has a maximum operating pressure of 2.7 MPa at a temperature of 177°C. Pressure is measured with capacitive-type electronic pressure transducers, and temperatures at the test section inlet and exit are measured with sheathed thermocouples in the flow streams. Boiling fluid pressure is set in the facility by adjusting

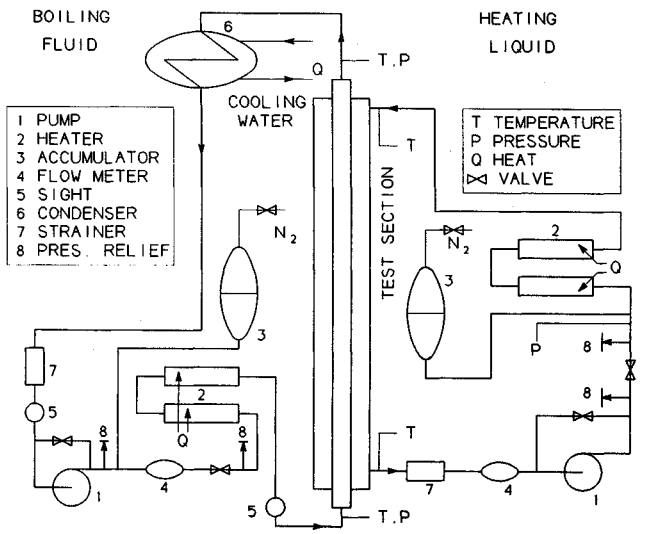

Fig. 1 Flow boiling facility.

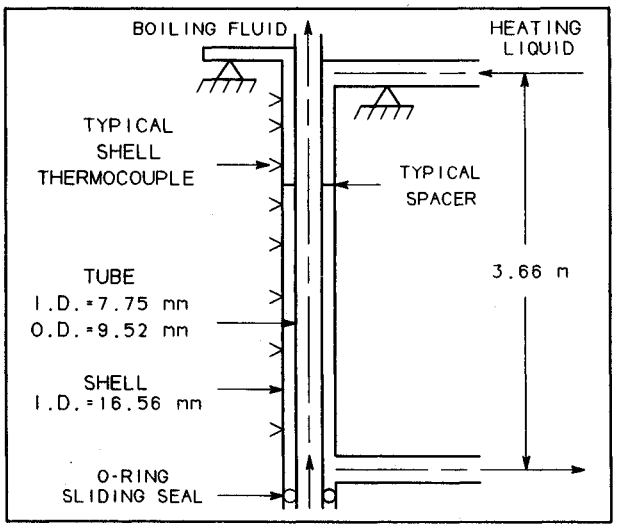

Fig. 2 Test section schematic.

the nitrogen pressure to the bladder-type accumulator. During steady-state testing, the accumulator system maintained the pressure very stable with variation of less than 3 kPa over a period of the order of 1 min. The turbine flow meters used in both fluid circuits have a turndown of 20 to 1 with an accuracy of better than 2%. All sensor outputs are read by a computer-controlled data acquisition system (DAS) in which 80 system and test section sensor voltages are read in less than 2 s, which is considerably faster than the system induced pressure fluctuation period of 1 min. Thus, the measurements were essentially uninfluenced by system disturbances.

The heating fluid circuit shown in Fig. 1 has the same operating pressure and temperature limits as the boiling fluid circuit of 2.7 MPa and 177°C, respectively. The heating fluid pressure necessary to maintain the liquid state was set with nitrogen pressure to the accumulator. Heat was supplied by a series arrangement of electric resistance heaters with a total power capability of 12 kW. Low heat flux of the final heaters in the series was used to avoid boiling of the heating fluid.

The test section shown in Fig. 2 was configured as a concentric single tube heat exchanger operating in the counter flow mode with water in the liquid state flowing in the annulus providing heat to boil R-12 flowing upward in the tube. This temperature-controlled arrangement produced a variable axial heat flux, and it limited the vapor superheat to the temperature of the heating fluid (water) at any location along the test section. A low wall-superheat was maintained in the test section typical of heat exchanger conditions.

The test section material was copper with tube inside diameter of 7.75 mm, tube wall thickness of 0.885 mm, and annulus outer diameter of 16.56 mm. The heated test section length of 3.66 m produced a large length-to-tube diameter ratio of 457, which allowed testing of the full post-CHF region at low wall-superheat at mass fluxes typical of once-through evaporator operation. The heating fluid temperature distribution along the test section was obtained from 57 thermocouples spot-welded to the shell (outer wall of the annulus tube) as discussed in the next section. Spacers were intermittently located along the test section length to maintain concentricity with minimal flow disturbance to the heating fluid. The shell was covered with a 50 mm thick layer of insulation, and the small heat loss through it was experimentally determined and included in the data reduction.

Data Acquisition and Reduction

Steady-state conditions, determined from analog recordings of test section stream temperatures and flow rates, were established at prescribed test parameters. Data were then accumulated on computer disk for later processing. A data scan consisted of measurements of the 57 shell thermocouples plus

10 measurements each of all flow rates, pressures, and test section stream thermocouples. The 10 measurements were averaged for each sensor in the post-test data reduction to eliminate any electronic noise that might be present. The shell thermocouples were not averaged because CHF movement would seriously affect the accuracy in the post-CHF region. The shell thermocouple readings were taken in less than 2 s as discussed previously, and the time for a complete data scan and data transfer to the computer was 25 s. These data constituted a single test, and the short time period required to obtain all of the data aided the maintenance of very steady conditions throughout. Other parameters along the length of the test section were calculated from these data after testing was completed.

The local heat flux in a liquid-heated system is calculated from shell temperature measurements and the heating fluid flow rate and properties. Several options are available, and results of a detailed investigation of many of them[8] showed that a relatively straightforward approach will provide good accuracy in the post-CHF region where axial heat flux gradients are not large. This approach (gradient method I) was utilized in the present study after the shell temperature measurements were smoothed with cubic splines. The heat flux to the boiling fluid at the tube inside surface q was calculated from the gradient of the shell temperatures as

$$q'' = \frac{m_h C_{p,h}}{\pi D_i} \frac{dT_s}{dZ} \tag{1}$$

The wall temperature of the outside of the boiling fluid tube T_o was calculated from

$$q'' = \frac{h_o D_o}{D_i} (T_s - Tw_o) \tag{2}$$

The annulus heat transfer coefficient at the boiling tube h_o was determined experimentally using the Wilson plot technique for a series of experiments performed with R-12 in the liquid state. The Monrad correlation[9] was found to represent the annulus data well, and it was used in the analysis of the subsequent boiling tests. The Monrad correlation is

$$\frac{h_o(D_s - D_o)}{k_h} = 0.02\, Re_h^{0.8}\, Pr_h^{1/3} \left(\frac{D_s}{D_o}\right)^{0.53} \tag{3}$$

A sensitivity check was performed on the use of Monrad's equation. The annulus heat transfer coefficient was reduced by 15% from the correlation value, and the data were reanalyzed. No significant change resulted in the post-CHF region, where the controlling thermal resistance is in the boiling fluid. Thus, the accuracy of the Monrad correlation for this application was verified.

Other data controls included test section heat balance calculations for the liquid R-12 tests as well as every boiling test where a substantial exit vapor-superheat was measured by a stream thermocouple indicating that thermal equilibrium had been achieved. These heat balances were within ±5% and mostly less than ±2%. The calculations were made using temperatures and flows measured by the DAS and constitutued an end-to-end calibration verification.

After the heat flux was determined in a boiling test, the boiling fluid enthalpy and equilibrium quality were calculated along the test section length from a heat balance. The boiling fluid equilibrium temperature was found from the pressure and enthalpy. The tube wall temperature at the inside surface Tw_i was found from a one-dimensional (radial) conduction model for the tube, and the equilibrium heat transfer coefficient was then determined based on this temperature and the boiling fluid saturation temperature. This procedure was followed for 10 tests covering the mass flux range of 182 to 808 kg/m²s. The reduced data are given in Fig. 3, and a typical

Z m	q" kW/m²	Tw_i C	X_{eq}	h_{eq} kW/m²C	Z m	q" kW/m²	Tw_i C	X_{eq}	h_{eq} kW/m²C
2.52	7.6	78.6	0.998	0.20	2.59	4.7	70.8	0.983	0.16
2.56	7.6	79.2	1.001	0.20	2.63	4.7	70.9	0.986	0.16
2.59	7.6	79.3	1.006	0.20	2.66	4.7	70.9	0.990	0.16
2.63	7.6	79.4	1.010	0.20	2.70	4.7	71.0	0.994	0.16
2.66	7.6	79.6	1.015	0.21	2.73	4.7	71.1	0.997	0.16
2.70	7.6	79.7	1.019	0.21	2.77	4.7	71.2	1.001	0.16
2.73	7.6	79.8	1.023	0.21	2.80	4.7	71.3	1.005	0.16
2.77	7.6	79.9	1.028	0.22	2.84	4.7	71.4	1.009	0.16
2.80	7.6	80.1	1.032	0.22	2.87	4.7	71.5	1.012	0.16
2.84	7.6	80.2	1.036	0.22	2.91	4.7	71.5	1.016	0.17
2.87	7.6	80.3	1.041	0.23	3.02	4.7	71.8	1.027	0.18
3.02	7.6	80.8	1.058	0.25	3.09	4.7	72.0	1.035	0.18
					3.16	4.7	72.1	1.042	0.19
					3.23	4.7	72.3	1.049	0.20
					3.30	4.7	72.5	1.057	0.21
G=0.254 Mg/m²s, X_{CHF}=0.991					G=0.182 Mg/m²s, X_{CHF}=0.963				
P=0.9806 MPa, Z_{CHF}=2.49 m					P=0.9806 MPa, Z_{CHF}=2.52 m				
2.56	6.4	70.4	0.959	0.21	2.56	10.2	87.9	0.995	0.22
2.59	6.4	70.6	0.963	0.21	2.59	10.2	88.1	0.999	0.22
2.63	6.4	70.7	0.968	0.21	2.63	10.3	88.2	1.003	0.22
2.66	6.4	70.8	0.972	0.21	2.66	10.3	88.3	1.007	0.22
2.70	6.4	70.9	0.977	0.21	2.70	10.3	88.4	1.011	0.23
2.73	6.4	71.0	0.982	0.21	2.73	10.3	88.6	1.015	0.23
2.77	6.4	71.1	0.986	0.21	2.77	10.3	88.7	1.019	0.23
2.80	6.4	71.2	0.991	0.21	2.80	10.4	88.8	1.023	0.23
2.84	6.4	71.3	0.995	0.21	2.87	10.4	89.1	1.031	0.24
2.87	6.4	71.4	1.000	0.21	2.95	10.5	89.3	1.039	0.25
2.98	6.4	71.7	1.013	0.22	3.02	10.5	89.5	1.048	0.26
3.09	6.4	72.1	1.027	0.23	3.09	10.6	89.8	1.056	0.27
G=0.202 Mg/m²s, X_{CHF}=0.947					G=0.368 Mg/m²s, X_{CHF}=0.984				
P=0.9802 MPa, Z_{CHF}=2.49 m					P=0.9806 MPa, Z_{CHF}=2.49 m				
2.20	28.9	106.3	0.915	0.44	2.10	37.2	107.5	0.811	0.56
2.24	28.9	106.7	0.923	0.44	2.17	36.9	108.7	0.827	0.55
2.27	28.9	107.1	0.931	0.44	2.24	36.4	110.0	0.844	0.53
2.31	28.9	107.5	0.938	0.43	2.31	35.7	111.3	0.860	0.51
2.34	28.8	108.0	0.946	0.43	2.38	34.9	112.6	0.876	0.49
2.38	28.8	108.4	0.953	0.43	2.45	34.1	113.9	0.892	0.47
2.41	28.7	108.8	0.961	0.42	2.52	33.1	115.2	0.907	0.45
2.45	28.6	109.2	0.969	0.42	2.59	32.2	116.5	0.922	0.43
2.49	28.5	109.7	0.976	0.42	2.66	31.4	117.8	0.937	0.41
2.52	28.4	110.1	0.984	0.41	2.73	30.7	118.9	0.951	0.39
2.56	28.3	110.5	0.991	0.41	2.80	30.0	120.0	0.964	0.38
2.59	28.1	111.0	0.999	0.40	2.87	29.4	121.1	0.978	0.37
2.63	28.0	111.5	1.006	0.40	2.95	28.9	122.1	0.991	0.36
2.77	27.1	113.3	1.035	0.41	3.05	28.3	123.6	1.010	0.35
2.95	25.9	115.7	1.070	0.41	3.16	27.8	124.9	1.029	0.35
					3.26	27.4	126.2	1.048	0.35
G=0.543 Mg/m²s, X_{CHF}=0.899					G=0.635 Mg/m²s, X_{CHF}=0.790				
P=0.9802 MPa, Z_{CHF}=2.13 m					P=0.9806 MPa, Z_{CHF}=2.03 m				
1.74	51.3	109.5	0.701	0.75	1.21	39.4	117.9	0.633	0.52
1.81	50.8	111.3	0.720	0.73	1.32	39.3	119.3	0.655	0.50
1.92	49.7	114.0	0.748	0.68	1.43	39.2	120.8	0.678	0.49
2.03	48.0	116.9	0.775	0.64	1.53	39.1	122.2	0.700	0.48
2.13	46.0	119.8	0.801	0.58	1.64	38.9	123.7	0.722	0.47
2.24	44.0	122.6	0.826	0.54	1.74	38.8	125.1	0.744	0.46
2.34	42.4	125.2	0.850	0.50	1.88	38.6	127.1	0.773	0.45
2.45	40.9	127.6	0.873	0.47	2.03	38.3	129.0	0.802	0.44
2.56	39.7	129.8	0.895	0.45	2.17	38.2	130.8	0.831	0.42
2.66	38.7	131.9	0.917	0.43	2.31	38.0	132.7	0.860	0.41
2.77	37.8	133.9	0.938	0.41	2.45	37.8	134.6	0.888	0.40
2.87	37.0	135.8	0.959	0.39	2.59	37.6	136.4	0.916	0.39
2.98	36.4	137.6	0.979	0.38	2.73	37.4	138.2	0.945	0.38
3.09	36.0	139.3	0.999	0.36	2.87	37.3	140.0	0.973	0.38
3.19	35.6	140.9	1.019	0.37	3.02	37.2	141.8	1.001	0.37
3.30	35.3	142.5	1.039	0.37	3.16	37.1	143.6	1.028	0.38
3.40	35.1	144.1	1.058	0.37	3.30	37.1	145.3	1.056	0.39
G=0.779 Mg/m²s, X_{CHF}=0.680					G=0.765 Mg/m²s, X_{CHF}=0.618				
P=0.9818 MPa, Z_{CHF}=1.67 m					P=0.9671 MPa, Z_{CHF}=1.14 m				
1.04	40.4	119.5	0.614	0.52	0.82	27.6	133.2	0.460	0.30
1.18	40.4	121.5	0.643	0.50	0.97	27.9	134.4	0.480	0.30
1.32	40.3	123.3	0.673	0.49	1.11	28.5	135.6	0.500	0.30
1.46	40.3	125.2	0.702	0.48	1.25	29.4	136.7	0.521	0.31
1.60	40.2	127.1	0.731	0.47	1.39	30.5	137.7	0.543	0.32
1.74	40.2	128.9	0.761	0.46	1.53	31.9	138.8	0.565	0.33
1.88	40.3	130.7	0.790	0.45	1.67	33.4	139.8	0.589	0.34
2.03	40.3	132.6	0.819	0.44	1.81	34.8	141.0	0.613	0.35
2.17	40.4	134.4	0.848	0.43	1.96	36.0	142.4	0.639	0.36
2.31	40.5	136.2	0.878	0.42	2.10	37.0	143.8	0.665	0.36
2.45	40.6	138.0	0.907	0.42	2.24	37.8	145.3	0.691	0.36
2.59	40.8	139.8	0.936	0.41	2.38	38.6	146.9	0.719	0.36
2.73	41.0	141.6	0.966	0.41	2.52	39.3	148.6	0.746	0.36
2.87	41.2	143.3	0.996	0.40	2.70	40.0	150.8	0.782	0.36
3.02	41.5	145.1	1.025	0.41	2.87	40.4	153.2	0.818	0.36
3.16	41.7	147.0	1.055	0.43	3.05	40.7	155.6	0.854	0.35
					3.23	40.8	158.0	0.890	0.35
					3.40	40.8	160.6	0.926	0.34
G=0.795 Mg/m²s, X_{CHF}=0.587					G=0.808 Mg/m²s, X_{CHF}=0.445				
P=0.9668 MPa, Z_{CHF}=0.97 m					P=0.9674 MPa, Z_{CHF}=0.75 m				

Fig. 3 Experimental data.

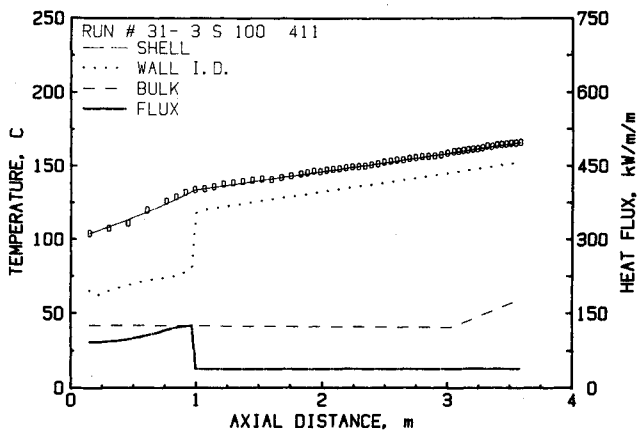

Fig. 4 Typical test section parameter distributions (G = 0.795 Mg/m²s, P = 0.9668 MPa).

plot is given in Fig. 4 in the direction of the boiling fluid flow. The open symbols shown in Fig. 4 represent the measured shell temperatures, and the solid line represents the cubic spline fit to them. The peak in the heat flux marks CHF. The boiling fluid temperature (bulk temperature in Fig. 4) is seen to be approximately constant at a saturation temperature of 41°C (in this and all other tests) until reaching superheat (under the condition of thermodynamic equilibrium) near the top of the test section at approximately 3 m beyond the inlet. Data for post-CHF regions are presented in Fig. 3 downstream of CHF extending through equilibrium qualities greater than unity in all but one test. The regions with $X_{eq} > 1.0$ are included because liquid drops may persist under nonequilibrium conditions. Data immediately downstream of CHF were not included if there was an indication of a transition boiling region based on the tube wall temperature; data near the top of the test section were not included to eliminate end effects.

Models and Correlations

The predictions of three equilibrium and six nonequilibrium models and correlations were compared to the R-12 post-CHF data. As noted previously, these models and correlations were chosen because of their good performance with low wall-superheat water data previously examined.

Equilibrium

Predictions from the Cumo correlation[10] and two forms of the Groeneveld correlation[11] were compared to the data of this study. All three post-CHF correlations are based on the assumption of thermodynamic equilibrium between phases and have the form of a single-phase vapor heat transfer correlation for turbulent flow with modifications to account for the presence of liquid drops. The form is given by

$$\frac{h_i D_i}{k_v} = aRe^b Pr_v^c \Gamma \tag{4}$$

The Reynolds number in Eq. (4) is for the vapor in the two-phase flow and is given by

$$Re = \frac{GD_i}{\mu_v}\left[X + S(1 - X)\frac{\rho_v}{\rho_l}\right] \tag{5}$$

The quality in Eq. (5) was based on equilibrium conditions, $X = X_{eq}$. The function Γ and constants a, b, and c in Eq. (4) were determined from comparison of the correlations with experimental data. Four forms of the Groeneveld correlation were developed using extensive data of the following types: (A) tube data with heat-flux-dependent term, (B) tube data without heat flux term, (C) tube and annuli data with heat flux term, and (D) tube and annnuli data without heat flux term. Correlations B and D were used in this study where Γ is a function of X_{eq} given by

$$\Gamma = \left[1 - 0.1\left(\frac{\rho_l}{\rho_v} - 1\right)^{0.4}(1 - X_{eq})^{0.4}\right]^d \tag{6}$$

The constants a, b, c, and d for the two cases are: Case (B), a = 0.00109, b = 0.989, c = 1.41 and d = −1.15; Case (D), a = 0.00327, b = 0.901, c = 1.32 and d = −1.50. The slip was taken as unity in Eq. (5).

Data from four laboratories were used in the development of the Cumo correlation.[10] The function Γ in Eq. (4) includes the quality at the critical heat flux, which was necessary to predict low quality data at high heat flux. The function is given by

$$\Gamma = \left(\frac{1 - X_{CHF}}{X_{eq} - X_{CHF}}\right)^{1/8} \tag{7}$$

The constants in the Cumo correlation are: a = 0.0089, b = 0.84, c = 1/3, and S = 1.0 in Eq. (5).

Nonequilibrium

Nonequilibrium correlations and models have been developed for post-CHF heat transfer for the condition of saturated liquid drops coexisting with superheated vapor. In this situation, the actual quality and the superheated vapor temperature are predicted in the process of determining heat transfer.

A distinction is made here between correlations, either empirical or including parameter groups of physical significance, and models in which some form of at least one conservation equation is solved. Post-CHF models rely on such solutions to predict the actual quality whereas correlations include nonequilibrium directly. Six nonequilibrium correlations and models were compared to the post-CHF data of this study.

Groeneveld-Delorme[12] developed a nonequilibrium correlation based on Eq. (4) from extensive data from which the actual quality was estimated. The function Γ in Eq. (4), which was used previously to include wall-to-drop heat transfer, was set to 1.0. The vapor Prandtl number and vapor thermal conductivity were evaluated at the film temperature. The actual quality and a slip of 1.0 were used in Eq. (5); the actual and equilibrium qualities are related by

$$\frac{X_{eq}}{X_a} = 1 + \frac{C_{p,v}(T_v - T_{sat})}{i_{lv}} \tag{8}$$

The constants for Eq. (4) are: a = 0.008348, b = 0.8774 and c = 0.6112. The correlation was completed essentially with an empirical relation for the actual quality that does not require knowledge of conditions at CHF. Care was taken in the development of this correlation to correctly predict asymptotic equilibrium conditions at qualities above 1.0 and at high mass fluxes.

Saha[13] developed two models for predicting heat transfer in the post-CHF region under nonequilibrium conditions. The form of Eq. (4) was used, and a differential equation for the conservation of mass of vapor was integrated from CHF to the point of interest in the post-CHF region. This equation related the actual quality to the equilibrium quality and utilized a correlation for the effectiveness of the vapor generation rate K1, which was developed from data. Thus, the first Saha model is termed K1. The second model was developed from the first in terms of the drop diameter at CHF, ζ_{CHF}. As with many correlations and models for high wall-superheat conditions, the Saha models do not explicity include direct wall-drop heat transfer in the formulations.

Among the many contributions to post-CHF heat transfer by Rohsenow and co-workers, a nonequilibrium correlation developed by Plummer et al.[7] considered the wall-drop heat transfer explicity, and it is the only correlation considered in

the present study that did so. The correlation superimposes wall-vapor and wall-drop heat transfer as

$$q'' = h_{w-v}(Tw_i - T_v) + h_{w-\delta}(Tw_i - T_{sat}) \quad (9)$$

The vapor-wall heat transfer was calculated from Eq. (4) with the actual quality used in Eq. (5). The constants used in Eq. (4) are: $a = 0.023$, $b = 0.8$, $c = 1/3$, and the function Γ is

$$\Gamma = \left(\frac{\mu_v}{\mu_{v,f}}\right)^{0.14}\left[1 + 0.3\left(\frac{D_i}{L_{CHF} + 0.01\,D_i}\right)^{0.7}\right] \quad (10)$$

where the vapor viscosity $\mu_{v,f}$ is evaluated at the film temperature. A relation developed for the actual quality from analysis and data employed different constants for three fluids: water, nitrogen, and R-12. The actual quality was defined in terms of the degree of nonequilibrium κ, where

$$\kappa = \frac{X_a - X_{CHF}}{X_{eq} - X_{CHF}} \quad (11)$$

and κ was correlated as

$$\kappa = C_1\,\ell n\left[G\left(\frac{D_i}{\rho_v\sigma}\right)^{0.5}(1 - X_{CHF})^5\right] + C_2 \quad (12)$$

The Plummer correlation did not include the assumption of homogeneous flow as did the other correlations considered; a relation was developed for slip with constants specific to the same three fluids given by

$$S = 1 + \frac{1}{2}\left[\frac{\left(\frac{\rho_l}{\rho_v}\right)^{0.205}}{\left(\frac{GD_i}{\mu_l}\right)^{0.016}} - 1\right]\left[1 - \frac{\kappa(X_{eq} - X_{CHF})}{1 - X_{CHF}}\right]^{\gamma} \quad (13)$$

where the exponent in Eq. (13) is $\gamma = A/\kappa^B$, and constants A and B are fluid-dependent.

The drop contribution to the heat transfer in the Plummer correlation was modeled as a function of void fraction and length from CHF. The Nusselt number based on $h_{w-\delta}$, the vapor thermal conductivity evaluated at the film temperature, $k_{v,f}$, and a characteristic dimension of 0.122 mm, was written as

$$Nu_{w-\delta} = (1 - \alpha)\exp\left(\frac{-2D_i}{L_{CHF}}\right) \quad (14)$$

Nishikawa[14] used two sets of data from short electrically-heated test sections to develop a nonequilibrium post-CHF model. Like the work of Saha, a differential equation for actual quality in terms of equilibrium quality was integrated down stream of CHF. Equation (4) was used with the actual quality in Eq. (5). The constants for Eq. (4) are: $a = 0.0048$, $b = 0.92$, $c = 0.4$ with Γ as

$$\Gamma = 1 + \frac{2}{(L_{CHF}/D_i)^{1.1}} \quad (15)$$

This model was developed from data with moderate wall-superheats by combining results from multiple tests, and it included large and small mass fluxes to account for conditions where the effects of nonequilibrium are small and large, respectively.

The final nonequilibrium correlation considered in this study was developed by Chen et al.[15] and is referred to as the CSO correlation. The correlation was based on the analogy between heat and momentum transfer. Several sets of data were used in the development of a relation between the actual and equilibrium qualities although measurements of vapor superheat were made by Chen subsequent to this development. The CSO correlation can be cast into the form of Eq. (4) using the actual quality and $S = 1.0$ in Eq. (5). The constants in Eq. (4) are: $a = 0.037/2$, $b = 0.83$, $c = 1/3$ and the function Γ is

$$\Gamma = \frac{X_a}{X_a + \frac{\rho_v}{\rho_l}(1 - X_a)} \quad (16)$$

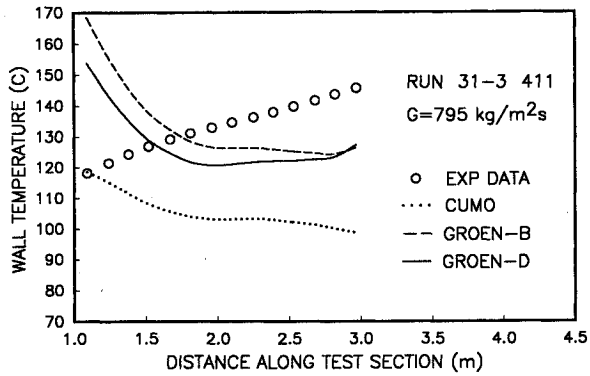

Fig. 5 Equilibrium correlation comparisons with Cumo[10] and Groeneveld[11] (T_{sat} = 41°C).

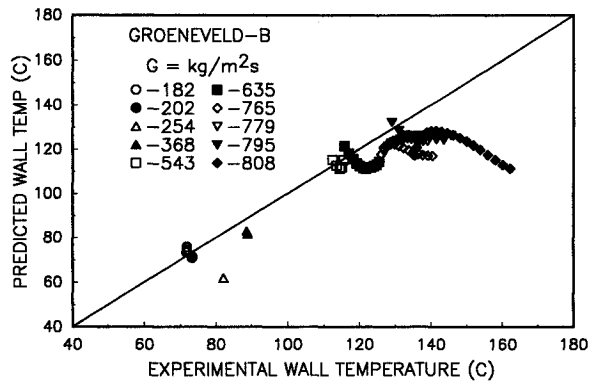

Fig. 6 Groeneveld[11] equilibrium correlation.

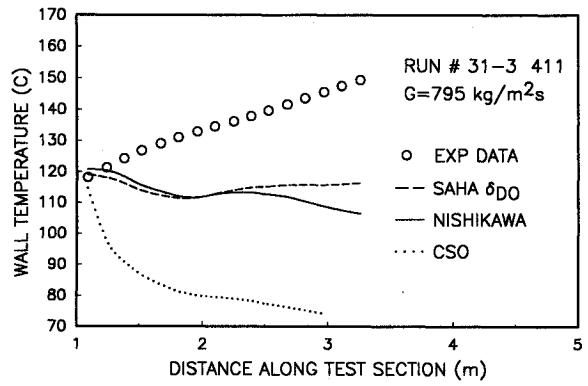

Fig. 7 Nonequilibrium correlation comparisons with Saha,[13] Nishikawa,[14] and Chen[15] (CSO).

Comparison of Results and Discussion

Equilibrium Correlations

The wall temperatures at the inside tube surface Tw_i from Fig. 4 are shown in Fig. 5 in the post-CHF region. The data of Fig. 5 are plotted up to $X_{eq} = 1.0$ and are compared to predictions from the three equilibrium correlations consid-

ered. The two Groeneveld correlations, GROEN-B and GROEN-D in Fig. 5, predict the average wall temperature of the data but have the opposite trend. The Cumo correlation also shows the opposite trend and poor magnitude prediction.

A comparison is given in Fig. 6 between all of the R-12 data from the present study and the Groeneveld-B correlation predictions. (The Groeneveld-D predictions were similar). Although the data trends were not predicted well, the comparison of Fig. 6 shows that the average wall temperatures of the data were predicted well except for the highest mass flux of the data. The wall temperature results of Fig. 6 show the same trends when converted to wall-superheats by subtracting the minimum axes temperature of 40°C, which approximately equals the R-12 saturation temperature of 41°C. The results for the Groeneveld correlations were similar for water data.[4]

Comparing all of the R-12 data to the Cumo correlation produced results similar to Fig. 5 where large differences existed over the entire mass flux range. The Cumo correlation predicted the magnitudes of the wall temperatures with better accuracy for the water data at mass fluxes below 1500 kg/m^{2}s. However, the differences for water data at higher mass fluxes were large as in the R-12 data at all mass fluxes.

Nonequilibrium Correlations and Models

The post-CHF data of Fig. 4 are plotted in Fig. 7 through an equilibrium quality of 1.055. Predictions of three nonequilibrium correlations and models shown in Fig. 7 do not predict the wall temperature magnitudes well, however, the trends of both the Saha and Nishikawa models are closer to the data than any of the equilibrium correlations considered.

The results shown in Fig. 8 using all of the R-12 data indicate that magnitude predictions with the best of these three correlations and models are not in good agreement with the data considering the entire mass flux range. (The results for both of the Saha models were similar to those of Fig. 8.) These results are similar to the comparisons with water data[4] where it was found that the nonequilibrium correlations predicted

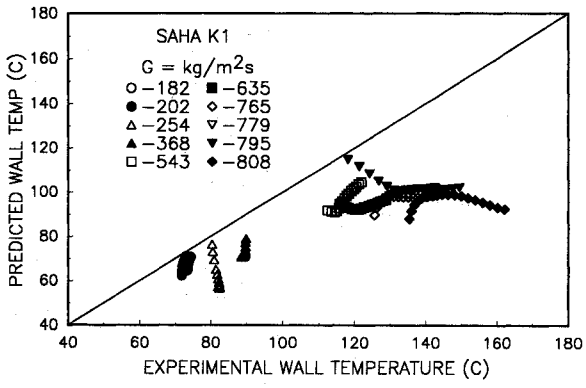

Fig. 8 Saha[13] nonequilibrium model.

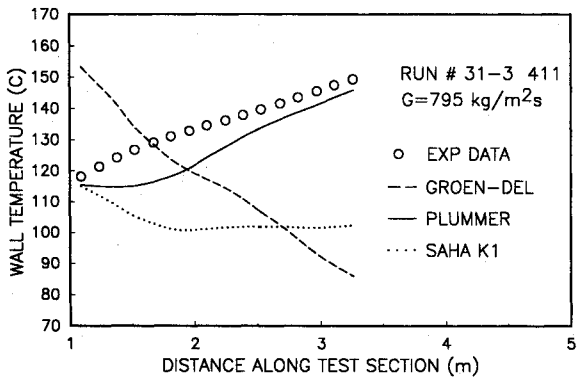

Fig. 9 Nonequilibrium correlation comparisons with Groeneveld,[12] Plummer,[7] and Saha.[13]

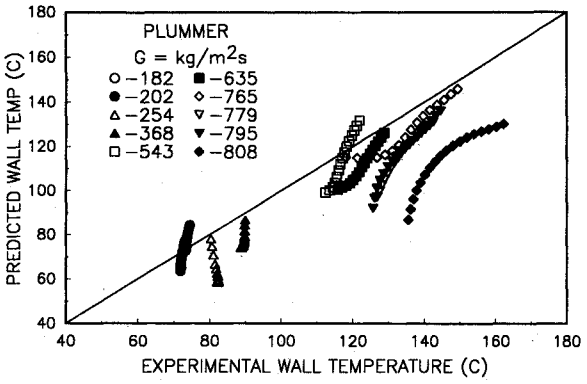

Fig. 10 Plummer nonequilibrium correlation.

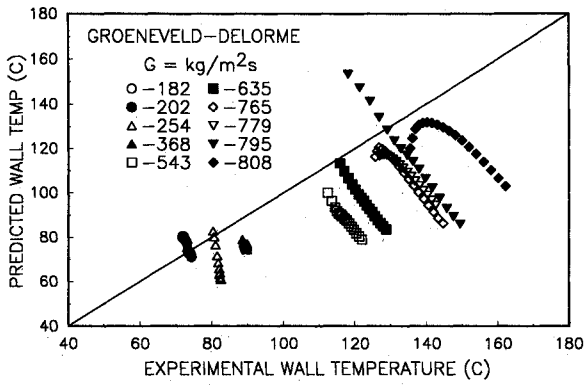

Fig. 11 Groeneveld-Delorme[12] nonequilibrium correlation.

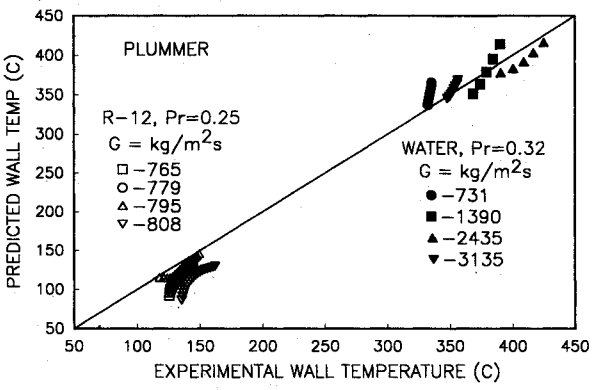

Fig. 12 Plummer[7] correlation with R-12 and water data at similar reduced pressures.

the data trends better than the equilibrium correlations although the magnitude predictions were not especialy good.

The final three nonequilibrium correlations and models are compared to post-CHF data along the test section in Fig. 9. It is clear that the Plummer correlation predictions are better than the others in both magnitude and trends. The data of Fig. 9 are typical of the data scatter as seen in Fig. 10 where all of the R-12 data are included. The data trends were predicted reasonably well by the Plummer, Saha, and Nishikawa equations; however, the accuracy was superior with the Plummer correlation as shown in Fig. 10. Agreement with the data is considered good over the range of mass fluxes tested except perhaps for the highest. In contrast, the magnitude of the Groeneveld-Delorme correlation predictions are seen in Fig. 11 to deviate from the data for most of the mass fluxes.

This important result, of the Plummer correlation clearly producing the best predictions of both magnitudes and trends of the R-12 data, was the same as found for the water data.[4] The Plummer correlation not only includes the phenomenon of thermodynamic nonequilibrium but it also incorporates an explicit model for direct wall-drop heat transfer. This heat

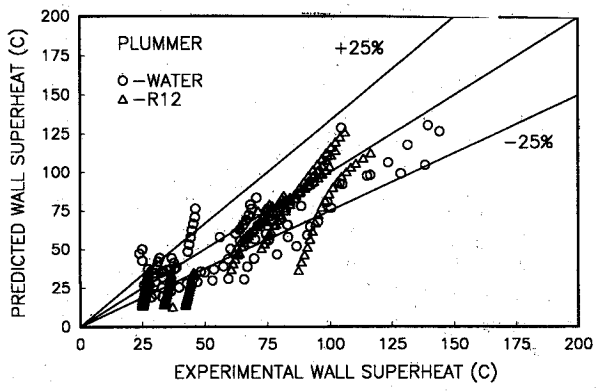

Fig. 13 Wall superheat predictions for all R-12 and water data.

transfer mechanism becomes more significant as wall-superheat is decreased, and although the magnitude of this contribution as predicted by the Plummer correlation was not large, it was an important factor influencing the good performance of the correlation.

Comparisons are shown between the Plummer correlation and both the R-12 and water data in Figs. 12 and 13. Data shown in Fig. 12 were chosen from the two fluid data sets at approximately the same reduced pressure. The higher mass fluxes of the R-12 data were chosen which overlapped with the lower range for the water data. The comparison of Fig. 12 is considered to be very good. The comparison of Fig. 13 is also good considering that the wall-superheat is plotted and all R-12 and water data are included. (Note that the majority of the data of Fig. 13 had wall-superheats below 100°C.)

The significance of nonequilibrium effects on the low wall-superheat data can best be assessed by considering all of the data for R-12 and water. The result that the nonequilibrium correlations generally predicted the data trends (but not necessarily the magnitudes) better than the equilibrium correlation was more pronounced with respect to the water data than the R-12 data of this study. The best data predictions considering both magnitude and trend and considering both R-12 and water data were from the Plummer correlation, which is a nonequilibrium correlation. These two results indicate that, although nonequilibrium effects are reduced for low wall-superheat, predictions are improved if it is included in the modeling.

Conclusions

Heat transfer data were obtained in the post-CHF region under heat exchanger conditions with low wall-superheat over a mass flux range important for once-through evaporator operation. Tests were performed with superheated vapor exiting the test section in order to include and assess the importance of thermodynamic nonequilibrium effects in the entire post-CHF region. Although the potential for nonequilibrium is reduced when the wall-superheat is low, the results indicated that this phenomena is still of enough importance that it should be included in modeling efforts.

The effect of direct heat transfer between liquid drops in the flow stream and the heated wall increases at low wall temperatures below the Leidenfrost temperature. Most correlations and models based on high wall temperature conditions have neglected this heat transfer. Based on the data comparisons with a variety of such equations, it was found that the wall-drop heat transfer had significant influence on the prediction of data trends. Although several correlations predicted the mean magnitudes reasonably well, good trend prediction only occurred when direct wall-drop heat transfer was included in the correlation.

Singularly, the best heat transfer predictions, of the trends and magnitudes of both the R-12 data of this investigation and the low wall-superheat water data,[5,6] were produced by the post-CHF correlation of Plummer et. al.[7] Low wall-superheat was common to both sets of data, but the fluids were different as were the mass flux, quality and reduced pressure ranges (with some overlap.) The Plummer correlation included the effects of both the phenomena of thermodynamic equilibrium and direct wall-drop heat transfer. Between the two fluids, the correlation performed well over a mass flux range of 182 to 3200 kg/m^{2}s and a reduced pressure range of 0.25 to 0.72 with wall superheats mostly below 100°C.

References

[1]Chen, J. C., "A Short Review of Dispersed Flow Heat Transfer in Post-Dryout Boiling," *Nuclear Engineering and Design,* Vol. 95, 1986, pp. 375–383.

[2]Wang, S. W., and Weisman, J., "Post-Critical Heat Flux Heat Transfer: A Survey of Current Correlations and Their Applicability," *Progress in Nuclear Energy,* Vol. 12, No. 2, 1983, pp. 149–168.

[3]Koai, K. K., Varone, A. F., Jr., and Rohsenow, W. M., "Comparison of Post Dryout Heat Transfer Prediction Methods," *USA-Japan Joint Symposium on Heat Transfer,* San Diego, 1985.

[4]George, C. M., and France, D. M., "Post-CHF Two-Phase Flow with Low Wall-Superheat," *Nuclear Engineering and Design,* Vol. 125, 1991, pp. 97–109.

[5]France, D. M., Carlson, R. D., Chiang, T., and Priemer, R., "Characteristics of Transition Boiling in Sodium Heated Steam Generator Tubes," *Journal of Heat Transfer,* Vol. 101, No. 2, 1979, pp. 270–275.

[6]France, D. M., Carlson, R. D., Chiang, T., and Minkowycz, W. J., "Critical Heat Flux Experiments and Correlation in a Long Sodium-Heated Tube," *Journal of Heat Transfer,* Vol. 103, No. 1, 1981, pp. 74–80.

[7]Plummer, D. N., Griffith, P., and Rohsenow, W. M., "Post-Critical Heat Transfer to Flowing Liquid in a Vertical Tube," *Transactions of the Canadian Society of Mechanical Engineers,* Vol. 4, No. 3, 1976–1977, pp. 151–158.

[8]Shin, S. K., and France, D. M., "Thermally Developing Flow in an Annulus with a Boiling Boundary," *Journal of Thermophysics and Heat Transfer,* Vol. 2, No. 3, 1988, pp. 235–241.

[9]Monrad, C. C., and Pelton, J. F., *Transactions of the American Institute of Chemical Engineers,* Vol. 38, 1942, p. 592.

[10]Cumo, M., and Urbani, G. C., "Post-Burnout Heat Transfer," CNEN/RT/ING, 1974.

[11]Groeneveld, D. C., and Gardiner, S. R. M., "Post-CHF Heat Transfer under Forced Convective Conditions," *Thermal and Hydraulic Aspects of Nuclear Reactor Safety,* Vol. 1, Light Water Reactors, Atlanta, GA, 1977, pp. 43–73.

[12]Groeneveld, D. C., and Delorme, G. G. J., "Prediction of Thermal Non-Equilibrium in the Post-Dryout Regime," *Nuclear Engineering and Design,* Vol. 36, 1976, pp. 17–26.

[13]Saha, P., "A Non-Equilibrium Heat Transfer Model for Dispersed Droplet Post-Dryout Regime," *International Journal of Heat and Mass Transfer,* Vol. 23, 1980, pp. 483–492.

[14]Nishikawa, K., Yoshida, S., Mori, H., and Takamatsu, H., "An Experiment on the Heat Transfer Characteristics in the Post-Burnout Region at High Subcritical Pressures," *Nuclear Engineering and Design,* Vol. 74, 1982, pp. 233–239.

[15]Chen, J. C., Ozkaynak, F. T., and Sundaram, R. K., "Vapor Heat Transfer in Post-CHF Region Including the Effects of Thermodynamic Non-Equilibrium," *Nuclear Engineering and Design,* Vol. 51, 1979, pp. 143–155.